STRESS CONCENTRATION IN ALUMINA/FIBRE EPOXY MODEL COMPOSITES

H. MAHIOU[1,2], A. BEAKOU[2] and R.J. YOUNG[1]
[1]*Manchester Materials Science Centre - UMIST Grosvenor Street*
Manchester M1 7HS, UK
[2]*Laboratoire de Recherches et Applications en Mécanique Avancée*
IFMA - B.P. 265 - F63175 Aubière Cedex - FRANCE

SUMMARY: In composite materials, fibre/fibre interaction phenomena due to fibre failure are crucial in determining the composite fracture behaviour. In this paper, we use the fluorescence spectroscopy to study the stress transfer and redistribution induced by fibre fracture in two-dimensional Nextel-610 fibres/epoxy-resin micro-composites. The stress along the fibres was mapped at different load levels and specimens with different inter-fibre distance were used to study the fibre content effect.
The experimental stress concentration factors (SCF) were smaller compared to values predicted from C_2SAC model. As expected the 2D configuration allows to access to the upper bound of the SCF in real composites. The measured SCF values agree well with those reported, in recent study, for carbon-fibre/epoxy model composites.

KEYWORDS: Stress transfer, Stress concentration factors, Model composites, Fluorescence spectroscopy, Raman spectroscopy, Stress concentrations, Alumina fibres, Interfacial shear stress.

INTRODUCTION

It is now well established that the strength of fibre-reinforced composites is determined by the strength distribution of embedded fibres and the local stress distributions caused by fibre fractures. Both the stress build-up in a broken fibre and the magnitudes and local distributions of stress in the intact fibres are governed by the material properties and by the fibre-matrix interface [1,2].
The problem of the local stress redistribution has been studied by a number of authors [3-9]. Mahiou and Béakou [10] have developed the C_2SAC model which allows the estimation of stress concentration factors as function of material properties and fibre volume fraction. The model is based on the micromechanical model of cell assembly.
Until recently, it was not possible to access the local stress field around fibre breaks experimentally. However, current developments in Raman spectroscopy allow for the *in situ* mapping of local stress in a fibre and, hence, the determination of stress concentrations in real composites [2,11-16].

In this paper, an experimental investigation into the influence of inter-fibre spacing on the stress transfer characteristics around fibre breaks, using the fluorescence spectroscopy technique, is conducted on Nextel-fibres/epoxy-resin 2D-microcomposite models. First, we describe the experimental procedure followed for the specimens preparation and the materials used. The results and discussion are then presented for samples with several inter-fibre spacings.

FLUORESCENCE SPECTROSCOPY

When a monochromatic light beam, such as laser, hits a molecule three phenomena can happen: absorption, emission or scattering. The absorption phenomenon is the basis of the infra-red technique, whereas the emission is used in the fluorescence technique. The scattering phenomenon is the basis of the Raman technique.

In this experimental investigation of stress transfer characteristics, use is made of Nextel-610 fibres, which are pure α-alumina fibres, embedded in epoxy matrix. For this kind of fibre, the fluorescence spectroscopy can be used. The basis of such technique is that the characteristic luminescence of the fibre shift with stress [17]. By using an optical microscope to define a probe of a few microns in diameter, the luminescence spectra can be obtained along the fibre. The observed shift in luminescence bands indicates the level of stress in the fibre.

The fluorescence of α-alumina fibres is due to the presence of Cr^{3+} impurities. These impurities give a doublet in the fluorescence spectrum, designated by R_1 and R_2 (Fig. 1), separated by about 30 cm^{-1}. The fluorescence signal is significantly more intense than a Raman signal and the band shifts are larger which leads to more accurate analysis.

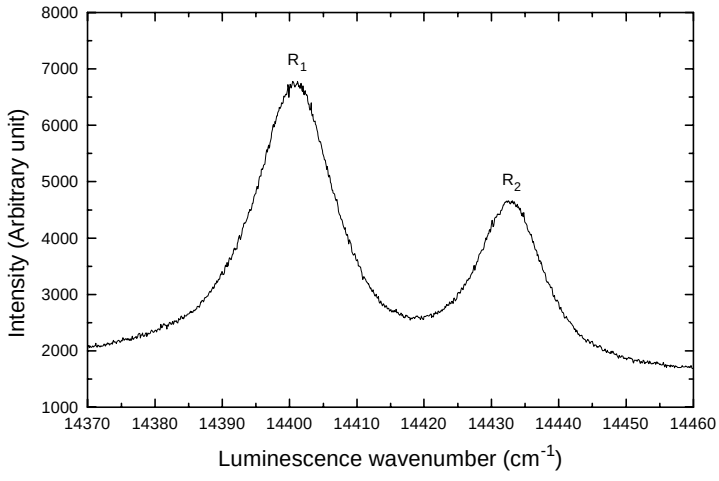

Fig. 1: *Luminescence spectrum of a Nextel fibre.*

Fluorescence spectroscopy can be performed using an unmodified Raman spectrometer. In this study, use was made of a double Raman spectrometer (SPEX 1403) shown schematically in figure 2.

EXPERIMENTAL PROCEDURE

Materials

The fibres used in this study were Nextel-610 fibres supplied by the company 3M, Minesota, USA. The fibres have an effective diameter of 12.8 μm and Young's modulus and tensile strength values of 380 GPa and 1.61 GPa, respectively [17].
The resin used was the two-part LY-HY 5052 (both supplied by Ciba-Geigy): Araldite® resin. The ratio of resin to hardener was 100:38 by weight. The resin was cured at room temperature for 24 hours and post-cured at 80°C for 8 hours. The resin has a tensile modulus of 3.0 GPa and a shear yield stress of 43 MPa [18].

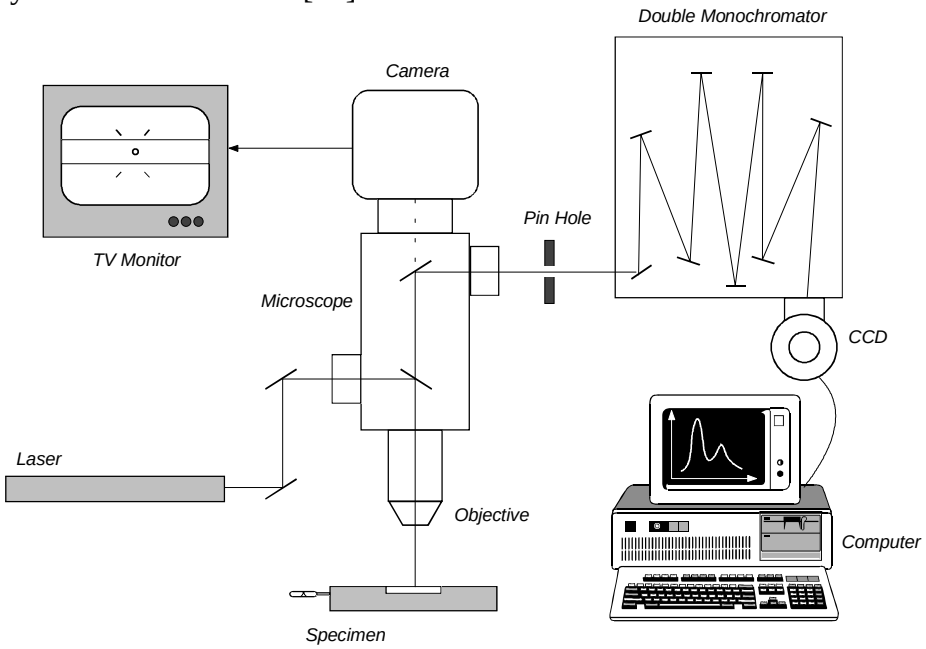

Fig. 2 *Schematic diagram of the Raman spectrometer*

Specimen preparation

Multi-fibre samples were prepared by positioning 3 fibres parallel at a predefined inter-fibre spacing using the technique developed by Wagner and Steenbakkers [19,20]. Three Nextel monofilaments were carefully extracted from a bundle and each fibre was guided in two corresponding slots on either side of the aligning apparatus (Fig. 3). A weight of 100 mg was attached to each fibre to hold the monofilament in position. Then, by rotating the slots the inter-fibre distance was adjusted. In the experiments three inter-fibre distances were used ($2.6\phi_f$, $5.4\phi_f$ and $12.3\phi_f$), where ϕ_f is the fibre diameter.

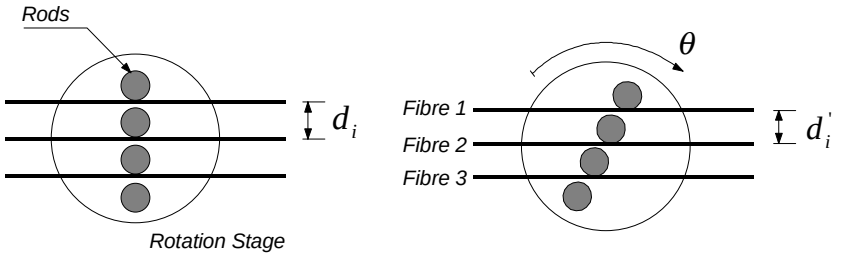

Fig. 3: *Illustration of the principle for varying the fibre-to-fibre distance*

After the inter-fibre distance was adjusted, the next step was to embed the fibres in epoxy. A silicone rubber mould was placed underneath the fibres on the mould supporting stage. The

stage was raised, lifting the mould until the fibres were at the centre of the half-depth of the mould. The fibres were glued in the cavity of a dumb-bell shaped silicone mould using fast-setting epoxy cement. Subsequently, degassed epoxy resin was carefully injected into the mould gradually from one side to the other. Finally, the samples were cured as described above. The cured specimens were then removed from the mould and polished with silicon-carbide paper. The inter-fibre distance was therefore measured using an optical microscope in order to obtain an average inter-fibre spacing for each specimen.

Fluorescence spectra acquisition

Luminescence spectra were obtained using an unmodified Raman microprobe system (Fig. 2). It is based upon a SPEX 1403 double monochromator connected to a modified Nikon optical microscope. The luminescence spectra were obtained using the 632.8nm line of a 15mW He-Ne laser. The Raman spectra were recorded using a charge-coupled device (CCD) cooled with liquid nitrogen and kept at 145K. The fluorescence peak positions were determined by fitting the raw data with two Lorentzian curves.

Strain/Stress calibration

In order to convert the shift of the fluorescence band into stress in the fibres, fluorescence spectra were obtained from Nextel fibres, bonded onto poly(methylmethacrylate) (PMMA) strips (3×10×60 mm) by a thin layer of PMMA, during deformation in a small four-point bending rig which fitted directly onto the microscope stage.

The variation of luminescence wavenumber for the R_2 band with applied strain is depicted in figure 4. It can be noticed that the luminescence R_2 band shifts approximately linearly both in tension and compression. A small non-linearity in the R_1 band shift has been reported elsewhere by Bin Yallee [17].

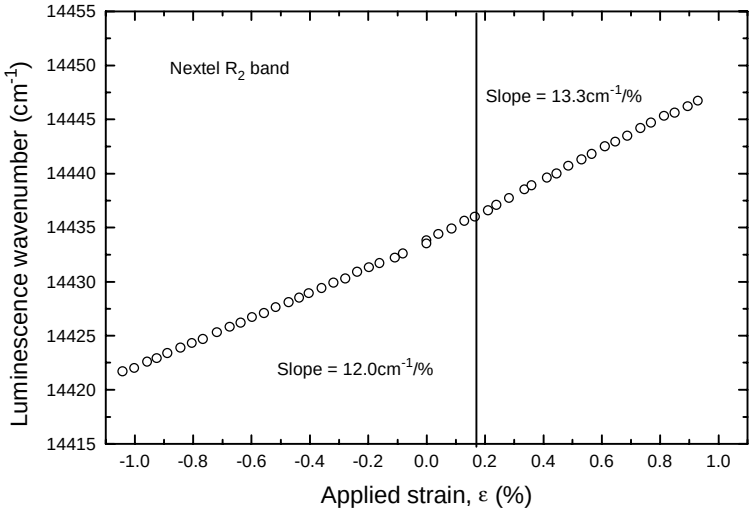

Fig. 4: *Variation of the wavenumbers of the luminescence R_2 band with applied strain for Nextel fibre [17].*

The stress profiles along a length of 1000 μm of each fibres making up the samples were recorded at increasing strain levels. The samples were loaded incrementally using a Minimat straining rig which was placed on to the stage of the Nikon microscope. A strain gauge was

attached onto the resin surface in order to obtain measurements of the applied strain to the sample.

Prior to the fibre fracture, spectra were taken at 50 μm intervals. Mapping of the fibre stress prior to fibre fracture was undertaken to ensure that the fibre stress closely follows the applied strain. Once a single fibre fracture was observed, the measurements were taken at 10 μm intervals in the vicinity of the break, at 20 μm intervals further away from the break, and at 50 μm intervals far away from the break. In all figures displayed in the next section, the fracture position along the fibre length is referred as x=0. The broken fibre was referred as **fibre 2** and the two intact neighbouring fibres were designated by **fibre 1** and **fibre 3.**

The fibre stress profiles are converted into interfacial shear stress distributions (ISS) by (a) fitting them, (b) calculating the derivatives from the equations of best fit, (c) deriving values of ISS by employing force balance acting upon the fibres and the interface [2]:

$$\tau = \frac{\phi_f}{2} \cdot \frac{d\sigma_f}{dx} \tag{1}$$

In the fitting procedure, continuity of shear stress was imposed. The stress concentration profile was determined by fitting a Gaussian distribution function to the stress profile of a fibre adjacent to a broken fibre. Subsequently the shear stress profiles along adjacent fibres were derived using equation (1).

RESULTS AND DISCUSSION

Figures 5 and 7 show the variation the fibre axial stress with distance along fibres in the microcomposites with large and small inter-fibre distance respectively at various strain levels (the strain levels are indicated in each figure).

Before fibre fracture

In figures 5-a and 7-a the variation of the stress profiles along the fibres at the zero strain level are displayed for the various samples. For all the specimens produced, an initial compressive stress of about 1.1 GPa can be seen. The initial stress is expected to develop during cooling of the composite from the processing temperature of 80°C due to the mismatch of thermal expansion coefficients between the matrix and fibre. A similar compressive stress for alumina-fibre/epoxy system has been reported elsewhere [17]. The values of residual stresses measured were also consistent with Nairn's analysis [17, 21]. Thus the application of stress must first of all overcome the initial compressive stress in the fibres before subjecting these to tension.

As the strain is increased to 0.37%, 0.46% and 0.42% for the specimens with large, intermediate and small inter-fibre distance, respectively, the fibres are in tension, see figures (5-b) and (7-b).

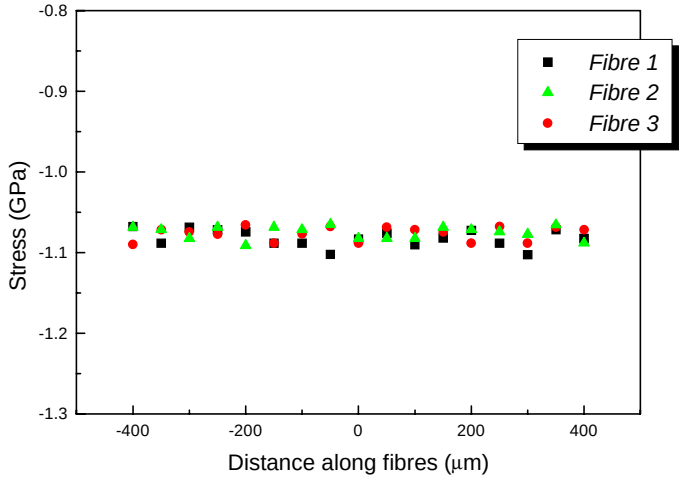

(a)

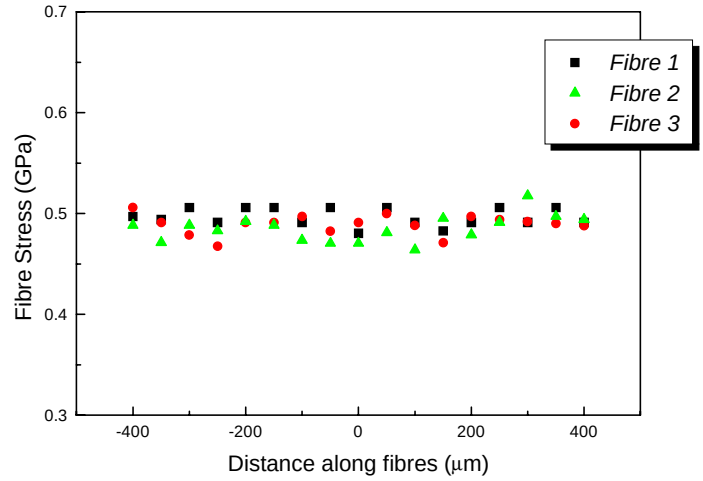

(b)

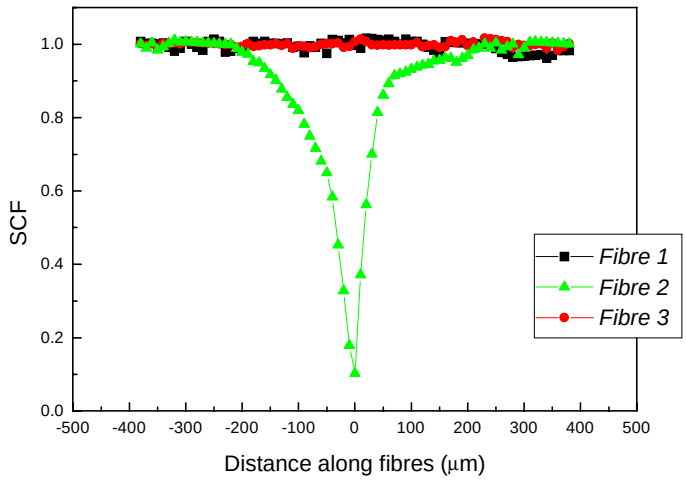

(c)

Fig. 5: *Stress profiles for a Nextel/epoxy microcompoites with large inter-fibre distance ($12.3\phi_f$); the applied strain is (a) 0%, (b) 0.36%,(c) 0.68%.*

After fibre fracture

At ε=0.68%, ε=0.72%, a break is observed in the middle fibre, respectively, for the large ($12.3\phi_f$) and small ($2.6\phi_f$) inter-fibre distance (Fig. 5-c and Fig. 7-c). Raman spectra were taken in the vicinity of the break as described above. Therefore, the stress distribution in both the fractured and the intact fibres could be obtained. Thus, single measurements at the vicinity of the fracture could yield: (a) *the ineffective length*, (b) the *interfacial shear stress* distribution in the fractured fibres, in addition to (c) *the positively affected length* and *the stress concentration factors* in the adjacent intact fibres.

It can be seen that the fibre stress drops to zero at the tip of the fibre break and then builds-up from either side to reach the maximum value of fibre stress at a distance of approximately 250μm. This length has been termed half of the ineffective length. Furthermore, figure 5-c clearly shows that over approximately 50μm to 70μm, around the break, linear stress build-up take place with a maximum interfacial shear stress around 38 MPa (Fig. 6). This shear stress is close to the shear yield stress of the epoxy-resin and hence, it is concluded that local yielding at the interface occurs behind the fibre break.

For the specimen with large inter-fibre distance no magnification of the stress level in fibre 1 and fibre 3 can be seen (Fig. 5-c). This suggests that at this inter-fibre spacing no over-stress of the intact fibres exists. In contrast for specimens with small and intermediate inter-fibre distances, the fibres 1 and 3 show a magnification of stress levels as a result of load redistribution (Fig. 7-c).

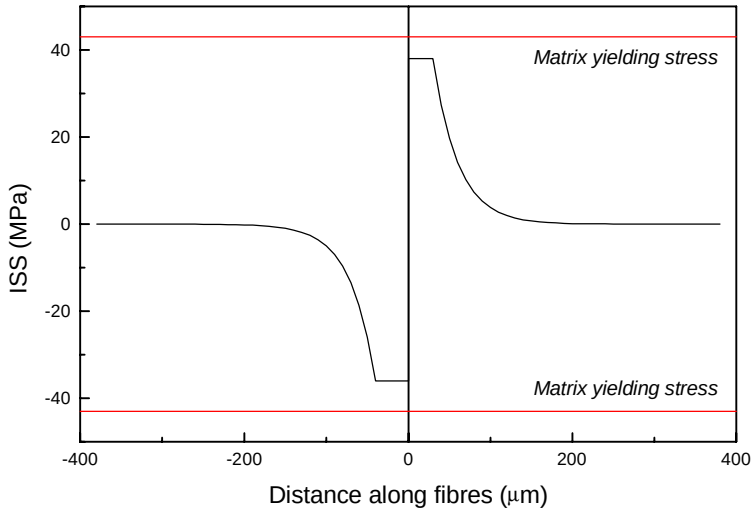

Fig. 6: *Derived interfacial shear stress along the broken fibre in figure 5-c for the specimen with large inter-fibre distance.*

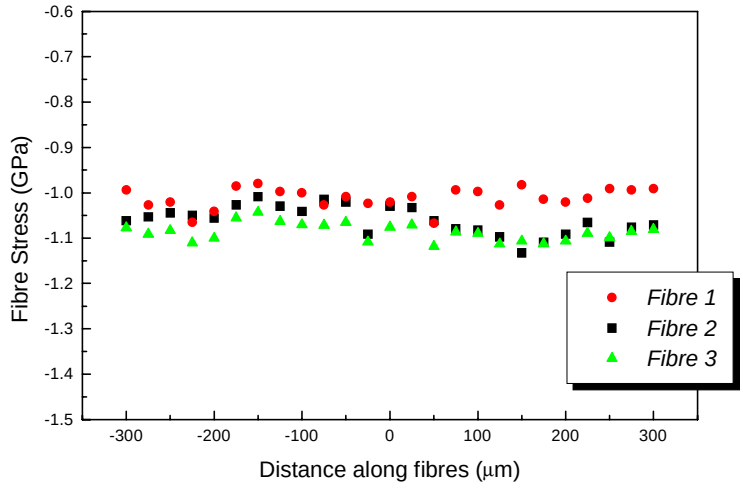

(a)

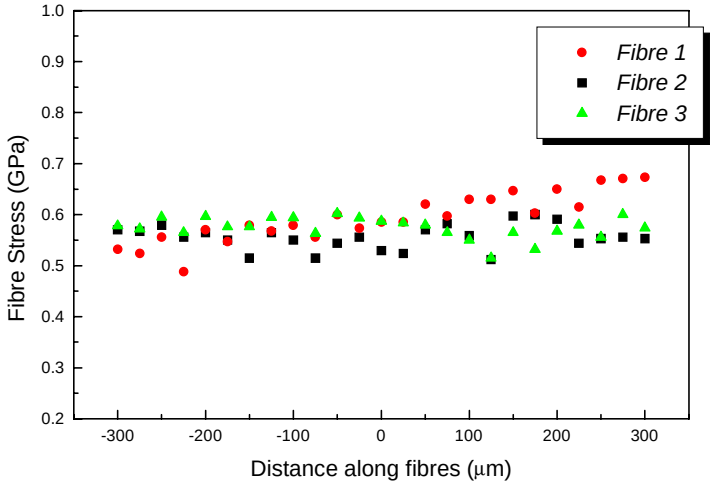

(b)

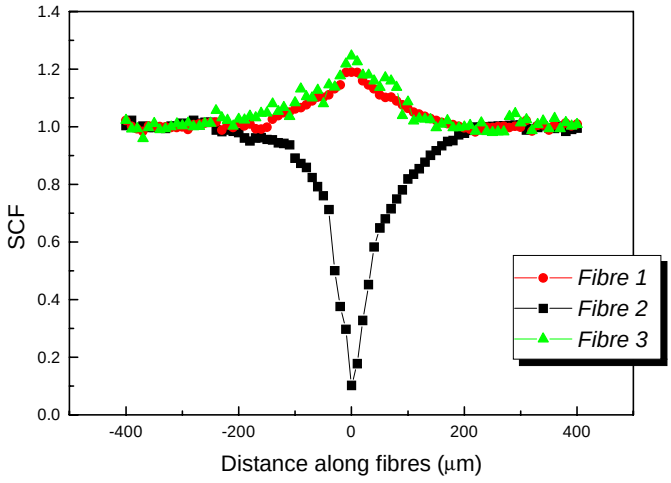

(c)

Fig. 7: *Stress profiles for a Nextel/epoxy microcompoites with small inter-fibre distance (2.6 ϕ_f); the applied strain is (a) 0%, (b) 0.42%,(c) 0.72%.*

Returning to the positively affected length, it is found that this length mirrors the ineffective length. Similar conclusions can be made for the specimen with intermediate inter-fibre

distance. The stress profile along the intact fibres is symmetrical and its maximum is situated in the rupture plane (Fig. 7-c).

After following the fitting procedure described above, the maximum of stress concentration factor was determined and is found to be 1.21 for $d_i = 2.6\phi_f$ and 1.10 for $d_i = 5.4\phi_f$. As shown in the reference [10], the SCF depends, for a fixed inter-fibre distance, upon the ratio E_f/E_m. For a carbon-fibre/epoxy-resin microcomposites (E_f/E_m=365/3), Van den Heuvel measured a stress concentration factor of 1.17±0.02 at an inter-fibre distance of $2.6\phi_f$ [20], see figure 8. This value is close to the one measured in our experiments. Such discrepancies could be due to ratio of the fibre to the matrix Young's moduli and to the small matrix crack observed near the fibre break. It was noticed however, that for the present composite system, the stress concentration factors decrease more rapidly with the inter-fibre distance than for Van den Heuvel's results [14].

For the Nextel-fibre/epoxy-resin composite (E_f/E_m=380/3) with an inter-fibre distance of $2.6\phi_f$ the C_2SAC model [10] predicts a SCF of 1.165. As expected the 2D configuration of the micro-composites used experimentally allows access to the upper bound of the stress concentration factor. Indeed, the C_2SAC model is based on square stitch arrangement of fibres [10]. It can be seen in figure 8, that the predicted values from the C_2SAC model tend asymptotically to 1.00 as the inter-fibre spacing increases.

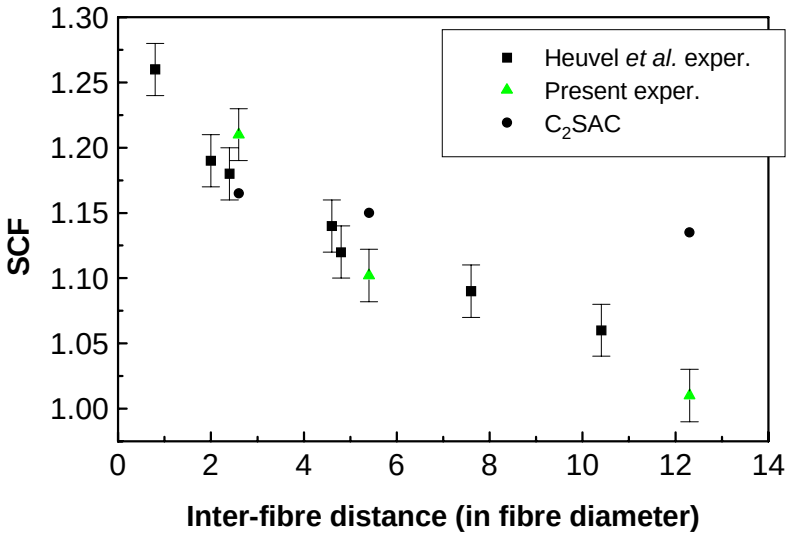

Fig. 8: *Stress concentration factors vs. the inter-fibre distance, comparison of the present measures with Van den Heuvel's results and the predicted values from our model.*

CONCLUSION

It has been shown that fluorescence spectroscopy can be used to determine the stress transfer characteristics near a fibre break. The stress concentration factor, the ineffective length and the positively affected length can be measured by means of the band shift of the fluorescence spectrum. For a series of micro-composites having inter-fibre spacing varying from $2.6\phi_f$ to $12.3\phi_f$, the SCF was found to decrease from a value of 1.21 at an inter-fibre distance of $2.6\phi_f$ to a value of unity at high inter-fibre distance ($12.6\phi_f$). These values obtained agree with those reported by Van den Heuvel. The measured values of the SCF has been compared to those calculated by our model. As expected the 2 dimensional configuration adopted for the micro-composites allows access to the upper bound of the stress concentration factors. The assumption made in Batdorf's model [22], used for the composite strength estimation, that the ineffective length mirrors the positively affected length has been proved experimentally.

REFERENCES

[1]-Mahiou, H. and Béakou, A. *Composites A*, 29A (1998), 1035.
[2]-Chohan, V. and Galliotis, C., *Comp. Sci. and Technol.*, **57** (1997), 1089.
[3]-Hedgepeth, J. M., *NASA TN D-882,* Langley Research Center,(1961).
[4]-Hedgepeth, J. M. and Van Dyke, P., *J. Comp. Mat.*, **1** (1967), 294.
[5]-Harlow, D. G. and Phoenix, S. L., *J. Comp. Mat.*, **12** (1978), 195.
[6]-Fukuda, H. and Kawata, K., *Fibre Sci. Tech.*, **9** (1976), 189.
[7]-Bader, M. G., Smith, R. L. and Pitkethly, M. J., *in Proc. Sixth Int. Conf. On Composite Materials (ICCM-6) and Second Europ. Conf. On Comp. Materials (ECCM-2)*, 20-24 July 1987, London, ed. F. L. Mattews, N. C. R. Buskell, J. M. Hodgkinson and J. Morton. Elsevier Applied Science, London, 1987, **Vol 5**, 481.
[8]-Case, S. W., Carman, G. P., Lesko, J. J., Fajardo, A. B. and Reifsnider, K. L., *J. Comp. Mat.*, **29** (1995), 208.
[9]-Wagner, H. D. and Eitan A., *Comp. Sci. Technol.*, **46** (1993), 353.
[10]-Mahiou, H. and Béakou, A., *Comp. Sci. Technol.*, **57** (1997), 1661.
[11]-Amer, M. A. and Schadler, L. S., *Comp. Sci. Technol.*, **57** (1997), 1129.
[12]-Martson, C., Gabbiatas, B., Adams, A., Marshall, P. and Galiotis, C., *Comp. Sci. Technol.*, **57** (1997), 913.
[13]-Paipetis, A. and Galliotis, C., *Comp. Sci. Technol.*, **57** (1997), 827.
[14]-Van Den Heuvel, P. W. J., Peijs, T. and Young R. J., *Comp. Sci. Technol.*, **57** (1997), 899.
[15]-Wagner, H. D., Amer, M. A. and Schadler, L. S., *J. Mat. Sci.*, **57** (1996), 1165.
[16]-Li, Z.-F., Grubb, D. T. and Phoenix, S. L., *Comp. Sci. Technol.*, **54** (1995), 251.
[17]-Bin Yallee, R., Young R. J., *Composites A*, in press.
[18]-Andrews, M. C., *Stress transfer in aramid/epoxy model composites*, PhD thesis, Victoria University of Manchester, (1994).
[19]-Wagner, H. D. and Steenbakkers, L. W., *J. Mat Sci*, **24** (1989), 3956.
[20]-Van den Heuvel , *An experimental and numerical investigation into failure phenomena in multi-fibre microcomposites*, PhD Thesis, Technische Universiteit Eindhoven, (1998).
[21]-Nairm, J. A., *Mechanics of Materials*, **13** (1992), 13.
[22]-Batdorf, S. B., *J. of Reinf. Plast. and Comp.*, (1982), 153.